Wide band-gap tuning $Cu_2ZnSn_{1-x}Ge_xS_4$ single crystals: optical and vibrational properties

E. Garcia-Llamas[a*], J. M. Merino[a], R. Serna[b], X. Fontané[c], I. A. Victorov[d], A. Pérez-Rodríguez[e], M. León[a], I. V. Bodnar[f], V. Izquierdo-Roca[b], R. Caballero[a*]

a. Photovoltaic Materials Group, Universidad Autónoma de Madrid, Departamento de Física Aplicada, C/ Francisco Tomás y Valiente 7, 28049 Madrid, Spain

b. Laser Processing Group, Instituto de Óptica, CSIC, C/ Serrano 121, 28006 Madrid, Spain.

c. Catalonia Institute for Energy Research, C/ Jardins de les Dones de Negre 1 2pl., 08930 Sant Adrià del Besòs-Barcelona, Spain

d. Institute of Physics of Solids and Semiconductors, Academy of Sciences of Belarus, 17 P. Brovka Str., 220072, Minsk, Belarus

e. IN2UB, Departament d'Electrònica, Universitat de Barcelona, C/ Martí i Franquès 1, 08028 Barcelona, Spain

f. Belarusian State University of Informatics and Radioelectronics, P. Browski Str., 6, Minsk 220013 Belarus

Corresponding Author*eduard.garcia@uam.es, Tel: +34 914973440, Fax: +34 914973969; raquel.caballero@uam.es, Tel: + 34 914978559

ABSTRACT. The linear optical properties of $Cu_2ZnSn_{1-x}Ge_xS_4$ high quality single crystals with a wide range of Ge contents (x = 0.1, 0.3, 0.5, 0.7, 0.9 and 1) have been investigated in the ultraviolet and near infrared range using spectroscopic ellipsometry measurements. From the analysis of the complex dielectric function spectra it has been found that the bandgap E_0 increases continuously from 1.49 eV to 2.25 eV with the Ge

content. Furthermore, the evolution of the interband transitions E_{1A} and E_{1B} has been also determined. Raman scattering using three different excitation wavelengths and its analysis have been performed to confirm the absence of secondary phases in the samples, and to distinguish between stannite, wurtzite, wurzstannite and kesterite structures. Additionally, the analysis of the high resolution Raman spectra obtained in samples with different [Ge]/([Ge]+[Sn]) ratios allows describing a bimodal behavior of the dominant A modes. The understanding of the incorporation of Ge into the Cu_2ZnSnS_4 lattice is fundamental in order to develop efficient bandgap engineering of these compounds towards the fabrication of kesterite based solar cells with enhanced performance.

KEYWORDS. $Cu_2ZnSn_{1-x}Ge_xS_4$ kesterite; Spectroscopic Ellipsometry; Raman scattering; Band-gap tuning; Solar cells.

1. Introduction

Nowadays, $Cu_2ZnSn(S,Se)_4$ (CZTSSe) compound is attracting special attention as a promising light absorber candidate for thin film solar cells because of its appropriated optical and electronic properties. Moreover, this compound is based on earth abundant and low toxic elements. However, the last record efficiency reported of 12.6% [1] is still very far away from the highest performance of $Cu(In,Ga)Se_2$ (CIGSe) solar cells, 21.7% [2]. One of the key of the success of CIGSe is the capacity of tuning the absorber band gap [3]. Recently, it has been shown that this band gap tuning can be also applied on CZTSSe by partially replacing tin with germanium [4,5] . The role of the Ge/Sn ratio in $Cu_2ZnSn_{1-x}Ge_x(S,Se)_4$ (CZTGSSe) is analogous to the Ga/In ratio in high efficient CIGSe solar cells. Moreover, there is an advantage in terms of reduction of costs by using the Ge/Sn pair instead Ga/In. Note that due to competition between the photovoltaic and the semiconductor and optoelectronics industries for the use of In and Ga resources, the price of the absorber could be very high [6]. Furthermore, the scarcity of In in the crust of earth might become a limitation in the near future in order to achieve the production of solar cells to cover the power annual demand by chalcopyrite thin film technology [7]. Improved efficiency of kesterite thin film solar cells has been already reported by replacing Sn with Ge, with device efficiencies of 9.4% [8]. In spite of this promising result for CZTGSSe compounds, there is not much known about their fundamental properties, and more particularly about the effect on the optical properties of the atomic ratio x = [Ge]/([Ge]+[Sn]). So far Morihama et al. [9] have reported information on structural properties of $Cu_2ZnSn_{1-x}Ge_xSe_4$ (CZTGSe) compounds by X-ray diffraction and determined the band gap energies by diffuse-reflectance spectra, and Grossberg et al. [10] have studied the recombination mechanisms of CZTGSe by

photoluminescence. In both cases, a linear increase of the bandgap from 0.9 eV to 1.3 eV at room temperature with the Ge content was shown. On another hand, there is even less information about the fundamental properties of $Cu_2ZnSn_{1-x}Ge_xS_4$ (CZTGS) compounds. A fundamental band gap energy E_0 = 2.2 eV and 2.0 eV for Cu_2ZnGeS_4 single crystal and single-crystalline nanowire arrays respectively have been reported in [11] and [12] respectively. Recently, E_0 = 1.59 and 1.90 eV have been determined for $Cu_2ZnSn_{0.9}Ge_{0.1}S_4$ and $Cu_2ZnSn_{0.5}Ge_{0.5}S_4$ single crystals respectively by spectroscopic ellipsometry [5]. The addition of Ge gives the possibility to control the bandgap of the absorber in a wider region from 1 to 2.3 eV, expanding the range of values available by varying the anion compositions in CZTSSe [13]. Moreover, it is expected for CZTGS compounds a linear decrease of the cell parameters when the Ge content increases, like the linear decrease reported in [9] for CZTGSe, which would control the lattice parameters depending on the Ge/Sn ratio. These are of main interest for the development of new multi-junction devices where photovoltaic conversion is optimized by improving the device efficiency in different spectral regions.

The objective of this work is to provide a thorough investigation of the optical, electronic and vibrational properties of $Cu_2ZnSn_{1-x}Ge_xS_4$ (CZTGS) single crystals as a function of the Ge content for a wide range of compositions, x= 0, 0.1, 0.3, 0.5, 0.7, 0.9 and 1 in a broad energy range from the near infrared to ultraviolet (0.8 eV to 4.6 eV). The composition of the crystals has been determined by energy dispersive X-ray (EDX) analysis. The dielectric constants for each selected composition were determined from variable angle spectroscopic ellipsometry measurements. This data were analysed to determine the fundamental band gap and the interband transition energies. Moreover, the near-surface region of every crystal has been studied by Raman spectroscopy. Raman spectroscopy is a technique based on the evaluation of the inelastic scattering process of molecules or crystals under monochromatic light. The evaluation of the energy of inelastic scattered photons in a crystalline material provides information on the vibrational energy and its density in the lattice (phonons) which is strongly sensitive to the atomic composition, crystal structure and crystal quality. As a result, Raman spectroscopy provides direct information of the chemico-physical properties of the material evaluated. For this reason, this technique is able to give reliable information about the crystalline structure and inhomogeneity on the surface. In this study three different wavelengths have been applied on the surface of the single crystals to be able to distinguish the presence of different secondary phases [14–16]. Additionally, the Raman characterization allowed evaluating the evolution of the Raman spectra with the [Ge]/([Ge]+[Sn]) ratio. The study of the vibrational properties on chacogenides solid solution systems such as Cu(S,Se)[17],$Cu(In,Al,Ga)(S,Se)_2$ [18–20],and $Cu_2(Fe,Zn)Sn(S,Se)_4$ [15,21,22] has demonstrated a high potential to evaluate the physical and chemical properties of the material such as the composition, crystal quality and presence of secondary phases, and opened the possibility of developing methodologies for non-destructive and high-accuracy compositional assessment.

2. Experimental

2.1. Synthesis of single crystals

$Cu_2ZnSn_{1-x}Ge_xS_4$ single crystals were synthesized by chemical vapor transport (CVT) of the elements [23]. Previously, several bulk kesterite compounds with different Ge/Sn ratios were grown by a modified Bridgman method, using constituents with purities ≥ 99.999%. The growth was carried out in an evacuated quartz ampoule introduced in a vertical furnace, followed by a heating ramp up to 1173 K avoiding overpressures. While the compound was liquid, a vibration movement was applied to the ampoule to improve the homogenization of the samples. The ampoule was then cooled down and an ulterior homogenization process was applied at 973 K for 7 days. The samples were grinded and used as source materials for the CVT synthesis.

The CVT process was performed in another quartz ampoule filled with the grown compound and adding 5 mg cm^{-3} of iodine, located in a furnace with two independent heating zones. Iodine was used as transport agent. The temperature at the crystallization zone was kept at 970 K, around 80 K lower than the temperature at the reaction zone (1050 K), and both were maintained for 8 days [5] . Varying the amount of Ge and Sn, seven $Cu_2ZnSn_{1-x}Ge_xS_4$ samples with x= 0, 0.1[5], 0.3, 0.5, 0.7, 0.9 and 1 were grown.

2.2.Characterization of $Cu_2ZnSn_{1-x}Ge_xS_4$ single crystals

The composition of the samples was measured by energy dispersive X-ray (EDX) (Oxford Instruments, model INCAx-sight) inside a Hitachi S-3000N scanning electron microscope. The measurements were performed at 25 kV operating voltage and the Cu-, Zn-, Ge-, S-K lines and Sn-L line were used. Table 1 shows the composition of the investigated samples. The relative error of the concentration values is 1% maximum.

To clarify the presence of secondary phases and to extract structural and vibrational information from the different CZTGS compounds, systematic Raman scattering measurements were carried out. The Raman spectra were obtained with a Horiba Jobin Yvon LabRam HR800-UV matched with an Olympus metallographic microscope. Backscattering measurements were done with three different excitation wavelengths (532, 325, and 785 nm) focusing the laser spot onto the single crystal, and orientating the excitation light polarization along the crystal grown direction. The use of different excitation wavelengths allows the selective enhance of the secondary phases modes and the activation of different CZTGS ones. The laser spot size is of the order of 1-2 μm, but in order to integrate the potential secondary phases, a spot raster facility that extends the analysis to an area of 30 μm x 30 μm has been used. In all Raman measurements, the power density for all excitation wavelengths has been kept below to 16kW/cm^2 to avoid thermal effects. All spectra have been calibrated using a Si single crystal as reference and imposing the Raman shift for the main Si band at 520 cm^{-1}. Simultaneous fittings of spectra with Lorentzian curves have allowed the identification of the peaks

attributed to their optical modes. The position of each Raman peak is presented in Table 2.

The measurement of the spectroscopic ellipsometry parameters ψ and δ of the crystals was carried out using a variable angle spectroscopic ellipsometer (Woollam VASE) at room temperature at three incidence angles of 60º, 65º and 70º, to ensure a consistent and accurate determination of the dielectric function, in the 0.75-4.5 eV photon energy range, using 0.03 eV steps. In order to obtain reliable data for the optical properties of the bulk crystals, the preparation of a good quality surface is extremely important to minimize the surface roughness and oxide formation effects [24,25]. Recently, we have observed the modification of the values of the effective transitions energies because of the presence of GeO_2 on the surface of these compounds [5]. Therefore, the crystal samples were thoroughly polished using a colloidal silica polishing suspension (Mastermet) in order to remove the oxides that might form at the surface, and the ellipsometric parameters ψ and δ were measured immediately after that. The complex effective dielectric function ($\varepsilon(E)= \varepsilon_1(E) + i\varepsilon_2(E)$) was determined by simulations with the WVASE ellipsometry analysis software assuming a two-phase (substrate-ambient) model [24,25]. The second derivative spectra of the real (ε_1) and imaginary part (ε_2) of the effective dielectric functions and their extrapolation have been used to determine the change of the fundamental band gap E_0 [11] as a function of the compositional changes, and the corresponding interband transitions E_{1A} and E_{1B} .

3. Results

CZTSSe-type compound can crystallize in two different structures, the stannite (space group I-42m) and the kesterite (space group I-4). These two structures are very similar with the only difference in the distribution of the cations in the tetrahedral sites [26]. This slight difference between these two crystallographic forms increases the difficulty to distinguish them. It is possible to determine the structure of these compounds by neutron diffraction experiments [27,28] but Raman spectroscopy measurements are also a powerful tool to distinguish between stannite and kesterite [15] and the chemicals inhomogeneity [14,16,17]. In this work, that technique was used to confirm the presence of a single phase material, so that the optical characterization could be carried out on the samples accurately.

Figure 1(a) shows the Raman spectra (in the region of 150-500 cm^{-1} and 650–750 cm^{-1}) obtained for Cu_2ZnSnS_4 (CZTS), $Cu_2Zn(Sn_{0.5}Ge_{0.5})S_4$ ($CZT_{0.5}G_{0.5}S$), and Cu_2ZnGeS_4 (CZGS) single crystals samples. Additionally, figure 1(b) shows the position of the main bands obtained under different excitation wavelengths, which are the more sensitive conditions in order to detect secondary phases. The Raman excitation using different wavelengths allows increasing the Raman cross-section efficiency of different compounds through the resonance or pre-resonant process. These processes enhanced several orders of magnitude the Raman contribution of the modes related to the phase that undergoes the resonant or pre-resonant effect. These processes occur when the

energy of the incident laser is coupled with the energy between the electronic ground energy level and other real electronic energy levels of the compound (resonant conditions) or close to this (pre-resonant condition). Applying these conditions is possible to select the proper excitation energy to detect low concentrations of secondary phases. This shows, Raman spectroscopy as a very sensitive technique, as reported for the CZT(S,Se) system [29–31] . Under 325 nm (3.8 eV), 532 nm (2.4 eV) and 785 nm (1.6 eV) excitation wavelengths, the ZnS [29], SnS_2 [32], Sn_2S_3[16,33], SnS [16,34], GeS [35] (direct band gaps of 3.7 eV, 2.5 eV, 2 eV, 1.4 eV and 1.6 eV, respectively) present resonant or pre-resonant conditions. $Cu_{2-x}S$ [17,36], GeS_2 [37], Cu_2SnS_3 [32,38,39], and Cu_2GeS_3 [40] phases do not show a resonant Raman scattering process under these excitation wavelengths because their band gap energies are not coupled with the excitation energy used. Nevertheless, the characteristic peaks of these secondary phases ($Cu_{2-x}S$, GeS_2, Cu_2SnS_3, and Cu_2Ge) are not overlapped with the main CZTGS peaks, and therefore the detection of these secondary phases is not compromised and could be detected at 532 nm excitation wavelength.

The application of the multiwavelength excitation methodology described by Dimitrievska et al. [41] based on the simultaneous fitting of the Raman spectra obtained under resonant, and non-resonant conditions (325, 532 and 785 nm excitation wavelengths) allows determining the characteristic peaks of CZTS, $CZT_{0.5}G_{0.5}S$ and CZGS samples. The comparison of the peak positions reported for kesterite [41,42], wurzite [43], and wurtztannite [44] crystal structures allows identifying the structure of the CZTGS system as kesterite type (Table 2). This result is in agreement with CZTS X-Ray diffractogram JCPDS 26-0575 database and the X-Ray diffractogram measured from the CZTS, $CZT_{0.5}G_{0.5}S$ and CZTGS single crystals powder samples (see Figure 2(a)). Figure 2(b) displays a zoom-in of the 112 peak, showing that all the samples are single phase. Moreover, Figure 1 shows the Raman spectra of the CZTGS compounds with the dominant peaks for each secondary phase. As it can be seen in Figure 1, there is no evidence of the presence of secondary phases in the CZTGS samples.

In order to evaluate the dependence of the dominant Raman contributions (A^1 and A^2 peaks) with the Ge content in the solid solution, Raman spectra of CZTGS single crystals samples with [Ge]/([Ge]+[Sn]) ratios close to 0, 0.3, 0.5, 0.7, 0.9 and 1 under 532 nm excitation wavelength have been measured (see figure 3). All these Raman spectra show the characteristic peaks of the kesterite structure, where A^1= 359 cm^{-1}, A^2= 296 cm^{-1} are the main modes of CZGS, and A^1 = 338 cm^{-1}, A^2 = 287 cm^{-1} are the main ones for CZTS.

Figure 4 shows the experimental spectral dependence of the dielectric functions of several $Cu_2ZnSn_{1-x}Ge_xS_4$ single crystals. The spectra exhibit several clear interband critical points (CP) structures analyzed in terms of standard analytic line shapes:

$$\varepsilon(\omega) = C - Aexp^{i\Phi}(\omega - E + i\Gamma)^m \quad (1)$$

where A is the amplitude, E is the energy threshold, Γ is the boarding, and Φ is the excitonic phase angle [25]. These parameters are determined by fitting the numerically obtained second derivative spectra $d^2\varepsilon(E)/dE^2$ of the experimental $\varepsilon(E)$ to equation (1). The exponent m has the value -½ for one-dimensional, 0 for two-dimensional, and ½ for three-dimensional critical points. From the CPs, information on the energy separation of valence and conduction bands can be obtained. Previously, calculations based on different features observed in complex dielectric constants have been reported in CZTS [45] and CZGS [11] bulk crystals. Here the $\varepsilon(E)$ spectra show three CPs structures: E_0, E_{1A} and E_{1B}.

To obtain the CP's energies, the $\varepsilon(E)$ spectra were smoothed by fast Fourier transform filtering before fitting $d^2\varepsilon(E)/dE^2$. Figure 5 exhibits the second derivatives of the real and imaginary parts of the dielectric functions and their fittings by using equation (1) of three samples. The fittings have been done taking into account CPs of 3D-type for the fundamental absorption edge $E_0=E_g$ and 2D-type for the second, E_{1A}, and third, E_{1B}, transition energies.

4. Discussion

Recently, Dhruba et al. [42] have reported the Raman evolution of the CZTGS kesterite type system. In [42], the reported Raman spectrum of CZTGS sample with a [Ge]/([Ge]+[Sn]) ≈ 0.5 shows a clear asymmetric and broad band centered at 347 cm^{-1}. This band has been assigned to pure chalcogenide S-S vibration, and their asymmetry and high FWHM have been attributed to the presence of the cationic disorder originated from the solid solution composition. In this work, the Raman spectrum obtained for a similar [Ge]/([Ge]+[Sn]) ratio (single crystal sample $CZT_{0.5}G_{0.5}S$) shows a splitting of such broad and asymmetric bands in two resolved contributions centered at 342 and 352 cm^{-1}. In order to evaluate the interpretation of this band splitting, the evolution of these two peaks with the x=[Ge]/([Ge]+[Sn]) ratio has been analyzed. Figure 3 shows the Raman spectra obtained for the different x=[Ge]/([Ge]+[Sn]) compositions from 275 to 380 cm^{-1} Raman shift. Increasing the Ge content results in a decrease in the intensity of the higher energy peak (lower Raman shift), while the intensity of the lower energy peak (higher Raman shift) increases. The Raman shift extrapolation of these two contributions at [Ge]/([Ge]+[Sn])=0 and 1 allows identifying the lower energy contribution as Sn-like peak, while the higher contribution one as Ge-like peak [46]. This indicates that as Germanium is incorporated in the CZTGS structure, the A mode shows a bimodal behavior. A detailed examination of the diffraction peaks for the $CZT_{0.5}G_{0.5}S$ sample (figure 2 (b)) does not show evidences of asymmetry or splitting of peaks that could be attributed to presence of mixed CZTGS kesterite compositions. This suggests that the Raman splitting of the A peak observed in the Raman spectra is intrinsic to the CZTGS solid solution.

Table 3 shows the energy threshold of the fundamental absorption edge $E_0 = 2.25$eV for Cu_2ZnGeS_4 (CZGS), which is in good agreement with the 2.27 eV of the kesterite CZGS theoretical calculations [26] and that obtained experimentally in single crystals

by ellipsometry [11]. This E_0 is assigned to the electronic transition at the Γ(000) point, corresponding to a direct transition from the valence-band maximum (VBM) to the conduction-band minimum (CBM). For the same compound, the energies of the second threshold E_{1A} and the third E_{1B} are 2.92 eV and 4.24 eV respectively. These energies are very close to that reported from theoretical band structure studies [26] for the transitions at the high critical points N(A): 2Π/a (0.5 0.5 0.5), T(Z): 2Π/a (0 0 0.5) and Γ_2:(0 0 0) of the first Brillouin zone for the E_{1A}, E_{1B} and E_0 transitions, respectively.

The partial substitution of Ge by Sn leads to a decrease of the E_0 values as displayed in Table 3. E_0 values of 2.20, 1.97, 1.90, 1.69, 1.59 and 1.51 eV were determined for Ge contents corresponding to x of 0.9, 0.7, 0.5, 0.3, 0.1 and 0, respectively. Figure 6 displays the variation of the fundamental energy E_0 with the experimental [Ge]/([Sn]+[Ge]) atomic ratio and its linear fitting. The band gap evolution follows Vegard's law, as already observed for $Cu_2ZnSn_{1-x}Ge_xSe_4$ [9].Theoretical works [26] suggest that Zn does not have an important role in the change of the band gap energy, so the deviation from a linear increase of E_0 with the Ge content may be related to the different Cu concentration of the samples. The reason of this deviation may be originated in the Cu-S p-d coupling that determines the VBM level, and the Cu-poor samples show higher band gaps due to the decrease in the VBM [26,47,48]. The phenomena of the "vacancy compound" for Cu-poorer thin films, increasing E_0, have been widely used in the chalcopyrite compound to improve their efficiency like in the case of CISe/CdS interface [49]. The composition of the kesterite plays an important role because the highest performance obtained for CZTSSe-based solar cells are obtained for Cu-poor kesterite layers.

In the case of E_{1A} and E_{1B}, values of E_{1A} of 3.04, 2.92, 2.82, 2.76 2.75, and 2,69 eV, and E_{1B} = 4.19, 4.20, 4.21, 4.10, 4.09, and 4.01 eV were obtained for x ≈ 0.9, 0.7, 0.5, 0.3, 0.1 and 0 respectively. To our knowledge, at present there are no available band structure calculations for these pseudo-quaternary compounds; however the same behavior as for CZTGS could be expected.

Following the band gap theoretical calculations [26,50], we can also conclude that our samples present a kesterite structure due to the fact that the stannite band gap is clearly smaller than those presented in this work. This result agrees with Raman and XRD measurements. Furthermore, it has been shown that spectroscopic ellipsometry is an excellent non-destructive technique to determine the band gap energy and to distinguish between kesterite and stannite structures. Additionally the presence of the energy band around 4eV at Γ point for all [Ge]/([Ge]+[Sn]) ratios is in agreement with the presence of an enhancement of the weaker Raman peaks by resonance process under 325nm (3.8 eV) as reported in [38] for the CZTS compound.

5. Conclusions

$Cu_2ZnSn_{1-x}Ge_xS_4$ single crystals with different x = Ge/([Ge]+[Sn]) atomic ratios were synthesized by chemical vapor transport. This work presents the wide band-gap tuning of CZTGS, varying E_0 from 2.25 to 1.51 eV when x changes from 1 to 0, as measured by spectroscopic ellipsometry. Raman scattering experiments have allowed the identification of the crystal structure of the CZTGS system with the kesterite type. Additionally, the Raman experiments performed on single crystals in the entire range of [Ge]/([Ge]+[Sn]) atomic ratios has allowed reporting the evolution of the A^1 and A^2 modes with the Ge incorporation on the CZTGS solid solution and describe the bimodal behavior of the A^1 in CZTGS kesterite solid solution system. This work shows an interesting perspective for the development and characterization of new multi-junction devices based on kesterites where the photovoltaic efficiency will be optimized by improving the device performance in different spectral regions by a suitable design of the absorber film composition.

6. Acknowledgements

This work was supported by the Marie Curie-ITN project (KESTCELL, GA: 316488), Marie Curie-IRSES project (PVICOKEST, GA: 269167), AMALIE (TEC2012-38901-C02-01) and SUNBEAM (ENE2013-49136-C4-3-R) project funded by the Spanish Ministry of Economy and Competitiveness. RC acknowledges financial support from Spanish MINECO within the Ramón y Cajal program (RYC-2011-08521).

7. References

[1] W. Wang, M.T. Winkler, O. Gunawan, T. Gokmen, T.K. Todorov, Y. Zhu, D.B. Mitzi, Device characteristics of CZTSSe thin-film solar cells with 12.6% efficiency, Adv. Energy Mater. (2013) 1–5. doi:10.1002/aenm.201301465.

[2] ZSW press release, ZSW, Pv Mag. (2014). http://www.pv-magazine.com/news/details/beitrag/zsw-sets-217-thin-film-efficiency-record_100016505/#axzz3LKgMy6rd.

[3] A.M. Gabor, J.R. Tuttle, D.S. Albin, M.A. Contreras, Noufi, Rommei, High-efficiency $CuIn_xGa_{1-x}Se_2$ solar cells made from $(In_x,Ga_{1-x})_2Se_3$ precursor films, Appl. Phys. Lett. 65 (1994) 198–200.

[4] G.M. Ford, Q. Guo, R. Agrawal, H.W. Hillhouse, Earth Abundant Element $Cu_2Zn(Sn_{1-x}Ge_x)S_4$ Nanocrystals for Tunable Band Gap Solar Cells: 6.8% Efficient Device Fabrication, Chem. Mater. 23 (2011) 2626–2629. doi:10.1021/cm2002836.

[5] R. Caballero, I. Victorov, R. Serna, J.M. Cano-Torres, C. Maffiotte, E. Garcia-Llamas, J.M. Merino, M. Valakh, I. Bodnar, M. León, Band-gap engineering of $Cu_2ZnSn_{1-x}Ge_xS_4$ single crystals and influence of the surface properties, Acta Mater. 79 (2014) 181–187. doi:10.1016/j.actamat.2014.06.040.

[6] S. Siebentritt, S. Schorr, Kesterites — a challenging material for solar cells, Prog. Photovoltaics Res. Appl. 20 (2012) 512–519. doi:10.1002/pip.2156.

[7] M.A. Green, Estimates of Te and In Prices from Direc Mining of Known Ores, Prog. Photovoltaics Res. Appl. 17 (2009) 347–359. DOI: 10.1002/pip.899.

[8] C.J. Hages, S. Levcenco, C.K. Miskin, J.H. Alsmeier, D. Abou-Ras, R.G. Wilks, M. Bär, T. Unold, R. Agrawal, Improved preformance of Ge-alloyed CZTGeSSe thin-film solar cells trhough control of elemental losses, Prog. Photovoltaics Res. Appl. 23 (2013) 376–384. doi:10.1002/pip.2442.

[9] M. Morihama, F. Gao, T. Maeda, T. Wada, Crystallographic and optical properties of $Cu_2Zn(Sn_{1-x}Ge_x)Se_4$ solid solution, Jpn. J. Appl. Phys. 53 (2014) 1–6.

[10] M. Grossberg, K. Timmo, T. Raadik, E. Kärber, V. Mikli, J. Krustok, Study of structural and optoelectronic properties of $Cu_2Zn(Sn_{1-x}Ge_x)Se_4$ (x=0 to 1) alloy compounds, Thin Solid Films. 582 (2014) 176–179. doi:10.1016/j.tsf.2014.10.055.

[11] M. León, S. Levcenko, R. Serna, G. Gurieva, A. Nateprov, J.M. Merino, E.J. Friedrich, U. Fillat, S. Schorr, E. Arushanov, Optical constants of Cu_2ZnGeS_4 bulk crystals, J. Appl. Phys. 108 (2010) 1–5. doi:10.1063/1.3500439.

[12] L. Shi, P. Yin, H. Zhu, Q. Li, Synthesis and Photoelectric Properties of Cu_2ZnGeS_4 and $Cu_2ZnGeSe_4$ Single-Crystalline Nanowire Arrays, Langmuir. 29 (2013) 8713–8717.

[13] J. He, L. Sun, S. Chen, Y. Chen, P. Yang, J. Chu, Composition dependence of structure and optical properties of $Cu_2ZnSn(S,Se)_4$ solid solutions: An experimental study, J. Alloys Compd. 511 (2012) 129–132. doi:10.1016/j.jallcom.2011.08.099.

[14] X. Fontané, L. Calvo-Barrio, V. Izquierdo-Roca, E. Saucedo, A. Pérez-Rodriguez, J.R. Morante, D.M. Berg, P.J. Dale, S. Siebentritt, In-depth resolved Raman scattering analysis for the identification of secondary phases: Characterization of Cu_2ZnSnS_4 layers for solar cell applications, Appl. Phys. Lett. 98 (2011) 1–3. doi:10.1063/1.3587614.

[15] X. Fontané, V. Izquierdo-Roca, E. Saucedo, S. Schorr, V.O. Yukhymchuk, M.Y. Valakh, A. Perez-Rodriguez, J.R. Morante, Vibrational properties of stannite and kesterite type compounds: Raman scattering analysis of $Cu_2(Fe,Zn)SnS_4$, J. Alloys Compd. 539 (2012) 190–194. doi:10.1016/j.jallcom.2012.06.042.

[16] X. Fontané, Doctoral Thesis, Caracterización por espectroscopia Raman para nuevas tecnologías fotovoltaicas Cu_2ZnSnS_4 para nuevas tecnologías fotovoltaicas, Universitat de Barcelona, 2013.

[17] M. Ishii, K. Shibata, H. Nozaki, Anion Distributions and Phase Transitions in $CuS_{1-x}Se_x$(x = 0-1) Studied by Raman Spectroscopy, J. Solid State Chem. 105 (1993) 504–511. doi:http://dx.doi.org/10.1006/jssc.1993.1242.

[18] V. Izquierdo-Roca, A. Shavel, E. Saucedo, S. Jaime-Ferrer, J. Álvarez-García, A. Cabot, A. Pérez-Rodríguez, V. Bermudez, J.R. Morante, Assessment of absorber composition and nanocrystalline phases in $CuInS_2$ based photovoltaic technologies by ex-situ/in-situ resonant Raman scattering measurements, Sol. Energy Mater. Sol. Cells. 95 (2011) S83–S88. doi:10.1016/j.solmat.2010.11.014.

[19] V. Izquierdo-Roca, X. Fontané, E. Saucedo, J.S. Jaime-Ferrer, J. Álvarez-García, A. Pérez-Rodríguez, V. Bermudez, J.R. Morante, Process monitoring of chalcopyrite photovoltaic technologies by Raman spectroscopy: an application to low cost electrodeposition based processes, New J. Chem. 35 (2011) 453–460. doi:10.1039/c0nj00794c.

[20] J. López-García, M. Placidi, X. Fontané, V. Izquierdo-Roca, M. Espindola, E. Saucedo, C. Guillén, J. Herrero, A. Pérez-Rodríguez, $CuIn_{1-x}Al_xSe_2$ thin film solar cells with depth gradient composition prepared by selenization of evaporated metallic precursors, Sol. Energy Mater. Sol. Cells. 132 (2015) 245–251. doi:10.1016/j.solmat.2014.09.003.

[21] M. Dimitrievska, G. Gurieva, H. Xie, A. Carrete, A. Cabot, E. Saucedo, A. Pérez-Rodríguez, S. Schorr, V. Izquierdo-Roca, Raman scattering quantitative analysis of the anion chemical composition in kesterite $Cu_2ZnSn(S_xSe_{1-x})_4$ solid solutions, J. Alloys Compd. 628 (2015) 464–470. doi:10.1016/j.jallcom.2014.12.175.

[22] M. Dimitrievska, H. Xie, A. Fairbrother, X. Fontané, G. Gurieva, E. Saucedo, A. Pérez-Rodríguez, S. Schorr, V. Izquierdo-Roca, Multiwavelength excitation Raman scattering of $Cu_2ZnSn(S_xSe_{1-x})_4$ ($0 \leq x \leq 1$) polycrystalline thin films: Vibrational properties of sulfoselenide solid solutions, Appl. Phys. Lett. 105 (2014) 031913. doi:10.1063/1.4891333.

[23] I. V. Bodnar, Growth and Properties of $CuAlS_{2x}Se_{2(1-x)}$ Single Crystals, Inorg. Mater. 38 (2002) 647–651. doi:10.1023/A:1016271804632.

[24] J.G. Albornoz, R. Serna, M. León, Optical properties and electronic structure of polycrystalline $Ag_{1-x}Cu_xInSe_2$ alloys, J. Appl. Phys. 97 (2005) 1–7. doi:10.1063/1.1899243.

[25] P. Lautenschlager, M. Garriga, S. Logothetidis, M. Cardona, Interband critical points of GaAs and their temperature dependence, Phys. Rev. B. 35 (1987) 9174–9189. doi:10.1103/PhysRevB.35.9174.

[26] S. Chen, X.G. Gong, A. Walsh, S.H. Wei, Electronic structure and stability of quaternary chalcogenide semiconductors derived from cation cross-substitution of II-VI and I-III-VI_2 compounds, Phys. Rev. B - Condens. Matter Mater. Phys. 79 (2009) 1–10. doi:10.1103/PhysRevB.79.165211.

[27] S. Schorr, H.-J. Hoebler, M. Tovar, A neutron diffraction study of the stannite-kesterite solid solution series, Eur. J. Mineral. 19 (2007) 65–73. doi:10.1127/0935-1221/2007/0019-0065.

[28] S. Schorr, The crystal structure of kesterite type compounds: A neutron and X-ray diffraction study, Sol. Energy Mater. Sol. Cells. 95 (2011) 1482–1488. doi:10.1016/j.solmat.2011.01.002.

[29] A. Fairbrother, V. Izquierdo-Roca, X. Fontané, M. Ibáñez, A. Cabot, E. Saucedo, A. Pérez-Rodríguez, ZnS grain size effects on near-resonant Raman scattering: optical non-destructive grain size estimation, CrystEngComm. 16 (2014) 4120–4125. doi:10.1039/c3ce42578a.

[30] A. Fairbrother, E. Garcia-Hemme, V. Izquierdo-Roca, X. Fontané, F.A. Pulgarin-Agudelo, O. Vigil-Galan, A. Perez-Rodriguez, E. Saucedo, Development of a Selective Chemical Etch To Improve the Conversion Efficiency of Zn-Rich Cu_2ZnSnS_4 Solar Cells, J. Am. Chem. Soc. 134 (2012) 8018–8021.

[31] S. López-Marino, Y. Sánchez, M. Placidi, A. Fairbrother, M. Espindola-Rodríguez, X. Fontané, V. Izquierdo-Roca, J. López-García, L. Calvo-Barrio, A. Pérez-Rodríguez, E. Saucedo, ZnSe etching of Zn-Rich $Cu_2ZnSnSe_4$: An oxidation route for improved solar-cell efficiency, Chem. - A Eur. J. 19 (2013) 14814–14822. doi:10.1002/chem.201302589.

[32] C. Julien, H.S. Mavi, K.P. Jain, M. Balkanski, C. Perez-Vicente, J. Morales, Resonant raman scattering studies of SnS_2 crystals, Mater. Sci. Eng. B. 23 (1994) 98–104. doi:http://dx.doi.org/10.1016/0921-5107(94)90341-7.

[33] H.R. Chandrasekhar, D.G. Mead, Long-wavelength phonons in mixed-valence

semiconductor $Sn^{II}Sn^{IV}S_3$, Phys. Rev. B. 19 (1979) 932–937.

[34] H.R. Chandrasekhar, R.G. Humphreys, U. Zwick, M. Cardona, Infrared and Raman spectra of the IV-VI compounds SnS and SnSe, Phys. Rev. B. 15 (1977) 2177–2183.

[35] J.D. Wiley, W.J. Buckel, R.L. Schmidt, Infrared reflectivity and Raman scattering in GeS, Phys. Rev. B. 13 (1976) 2489–2496.

[36] P. Kumar, M. Gusain, R. Nagarajan, Supporting Information Synthesis of $Cu_{1.8}S$ and CuS from Copper-Thiourea complexes ; anionic (Cl^- , NO_3^- , SO_4^{2-}) influence on the product stoichiometry, Inorg. Chem. 50 (2011) 3065–3070.

[37] Q. Wang, S.-Z. Kang, X. Li, Y.-W. Yang, L. Qin, J. Mu, A facile preparation of crystalline GeS_2 nanoplates and their photocatalytic activity, J. Alloys Compd. 631 (2015) 21–25. doi:10.1016/j.jallcom.2014.12.259.

[38] P.A. Fernandes, P.M.P. Salomé, A.F. da Cunha, Study of polycrystalline Cu_2ZnSnS_4 films by Raman scattering, J. Alloys Compd. 509 (2011) 7600–7606. doi:10.1016/j.jallcom.2011.04.097.

[39] D.M. Berg, R. Djemour, L. Gütay, G. Zoppi, S. Siebentritt, P.J. Dale, Thin film solar cells based on the ternary compound Cu_2SnS_3, Thin Solid Films. 520 (2012) 6291–6294. doi:10.1016/j.tsf.2012.05.085.

[40] D.B. Khadka, J. Kim, Study of structural and optical properties of kesterite Cu_2ZnGeX_4 (X = S, Se) thin films synthesized by chemical spray pyrolysis, CrystEngComm. 15 (2013) 10500–10509. doi:10.1039/c3ce41387j.

[41] M. Dimitrievska, A. Fairbrother, X. Fontané, T. Jawhari, V. Izquierdo-Roca, E. Saucedo, A. Pérez-Rodríguez, Multiwavelength excitation Raman scattering study of polycrystalline kesterite Cu_2ZnSnS_4 thin films, Appl. Phys. Lett. 104 (2014) 1–5. doi:10.1063/1.4861593.

[42] D.B. Khadka, J. Kim, Band Gap Engineering of Alloyed $Cu_2ZnGe_xSn_{1-x}Q_4$ (Q=S,Se) Films for Solar Cell, J. Phys. Chem. C. 119 (2015) 1706–1713. doi:10.1021/jp510877g.

[43] Y. Li, W. Ling, Q. Han, W. Shi, Colloidal $Cu_2Zn(Sn_{1-x}Ge_x)S_4$ nanocrystals: electrical properties and comparison between their wurtzite and kesterite structures, RSC Adv. 4 (2014) 55016–55022. doi:10.1039/C4RA10780B.

[44] M. Guc, A.P. Litvinchuk, S. Levcenko, V. Izquierdo-Roca, X. Fontané, M.Y. Valakh, E. Arushanov, A. Pérez-Rodríguez, Optical phonons in the wurtzstannite Cu_2ZnGeS_4 semiconductor: Polarized Raman spectroscopy and first-principle calculations, Phys. Rev. B. 89 (2014) 1–7. doi:10.1103/PhysRevB.89.205205.

[45] S. Levcenko, G. Gurieva, M. Guc, A. Nateprov, Optical constants of Cu_2ZnSnS_4 bulk crystals, Mold. J. Phys. Sci. 8 (2009) 173–177.

[46] R. Caballero, J.M. Cano-Torres, E. Garcia-Llamas, X. Fontané, A. Pérez-Rodríguez, D. Greiner, C. a. Kaufmann, J.M. Merino, I. Victorov, G. Baraldi, M. Valakh, I. Bodnar, V. Izquierdo-Roca, M. León, Towards the growth of $Cu_2ZnSn_{1-x}Ge_xS_4$ thin films by a single-stage process: Effect of substrate temperature and composition, Sol. Energy Mater. Sol. Cells. 139 (2015) 1–9. doi:10.1016/j.solmat.2015.03.004.

[47] S.H. Han, A.M. Hermann, F.S. Hasoon, H.A. Al-Thani, D.H. Levi, Effect of Cu deficiency on the optical properties and electronic structure of CuInSe2 and CuIn0.8Ga 0.2Se2 determined by spectroscopic ellipsometry, Appl. Phys. Lett. 85 (2004) 576–578. doi:10.1063/1.1776616.

[48] S. Levcenko, M. León, G. Gurieva, R. Serna, J.M. Merino, E.J. Friedrich, E. Arushanov, I. V. Bodnar, Comparative study of tetragonal $Cu_2In_7Se_{11.5}$ and trigonal $CuIn_5Se_8$ by spectroscopic ellipsometry, Mater. Chem. Phys. 125 (2011) 77–81. doi:10.1016/j.matchemphys.2010.08.074.

[49] D. Schmid, M. Ruckh, F. Grunwald, H.W. Schock, Chalcopyrite/defect chalcopyrite heterojunctions on the basis of $CuInSe_2$, J. Appl. Phys. 73 (1993) 2902.

[50] S. Chen, X.G. Gong, A. Walsh, S.H. Wei, Crystal and electronic band structure of Cu_2ZnSnX_4 (X=S and Se) photovoltaic absorbers: First-principles insights, Appl. Phys. Lett. 94 (2009) 1–3. doi:10.1063/1.3074499.

Table

Table 1. Composition of the single crystals measured by EDX.

Sample	Cu (at%)	Zn (at%)	Sn (at%)	Ge (at%)	S (at%)	Cu/(Zn +IV)	(Cu+Zn) /IV	Ge/IV	S/M
Cu_2ZnGeS_4	26.95	11.38	--	11.08	50.59	1.20	3.45	1.00	1.02
$Cu_2ZnSn_{0.1}Ge_{0.9}S_4$	24.81	11.78	0.85	9.80	51.32	1.09	3.43	0.92	1.08
$Cu_2ZnSn_{0.3}Ge_{0.7}S_4$	27.18	11.90	3.39	8.48	49.05	1.14	3.29	0.71	0.96
$Cu_2ZnSn_{0.5}Ge_{0.5}S_4$	24.62	12.07	5.63	6.77	50.91	1.01	2.96	0.55	1.04
$Cu_2ZnSn_{0.7}Ge_{0.3}S_4$	26.49	11.78	9.17	3.55	49.00	1.08	3.01	0.28	
$Cu_2ZnSn_{0.9}Ge_{0.1}S_4$	24.77	13.13	11.29	1.04	49.77	0. 97	3.07	0.08	0.99
Cu_2ZnSnS_4	24.48	12.13	12.71	--	50.68	0.98	2.88	--	1.02

Note: M= Cu + Zn + Sn + Ge; IV = Sn + Ge

Table 2 revised

Table 2. Frequency (in cm^{-1}) of the clear resolved peaks of Raman spectra measured in the regions 200-450 cm^{-1} and 650-750 cm^{-1}. These are compared to the experimental Raman shifts reported in CZTGS samples. **In bold are reported the excitation wavelengths (in nm) used in the Lorentzian curve fitting analysis**. Underlined are indicated the bands related to second order Raman scattering process.

CZTS Kesterite		CZTS wurtzite	$CZT_{0.5}G_{0.5}S$ Kesterite		$CZT_{0.5}G_{0.5}S$ wurtzite	CZGS Kesterite		CZGS Wurtzstannite	CZGS wurtzite
This work	[41]	[43]	This work	[42]	[43]	This work	[42]	[44]	[43]
325, 532, 785	**325, 532, 785**	**514**	**325, 532, 785**	**532**	**514**	**325, 532, 785**	**532**	**514 785**	**514**
166			153			157		161	
251	255		184			191		164	
263	263		256			262		178	
	271		270	270		274	273	184	
287	287		280			295	293	273	
302	302		292	292		315	315	277	
317	316			314		339		289	
320			331			359	357	241	354
	332		343			382		314	
338	338	332		347	343	402	403	333	
347	347		352					362	
	353		367					383	
367	367		379					386	
374	374		391	395				407	
								418	
672			696			715			

Table

Table 3. Transition energies E_0, E_{1A} and E_{1B} values of $Cu_2ZnSn_{1-x}Ge_xS_4$ (x = 0.1, 0.3, 0.5, 0.7, 0.9 and 1).

Sample	E_0 (±0.03) (eV)	E_{1A} (±0.03) (eV)	E_{1B} (±0.03) (eV)
Cu_2ZnGeS_4	2.25	2.92	4.24
$Cu_2ZnSn_{0.1}Ge_{0.9}S_4$	2.20	3.04	4.19
$Cu_2ZnSn_{0.3}Ge_{0.7}S_4$	1.98	2.92	4.20
$Cu_2ZnSn_{0.5}Ge_{0.5}S_4$	1.90	2.82	4.21
$Cu_2ZnSn_{0.7}Ge_{0.3}S_4$	1.69	2.76	4.10
$Cu_2ZnSn_{0.9}Ge_{0.1}S_4$	1.59	2.75	4.09
Cu_2ZnSnS_4	1.51	2.69	4.01

Figure

Click here to download high resolution image

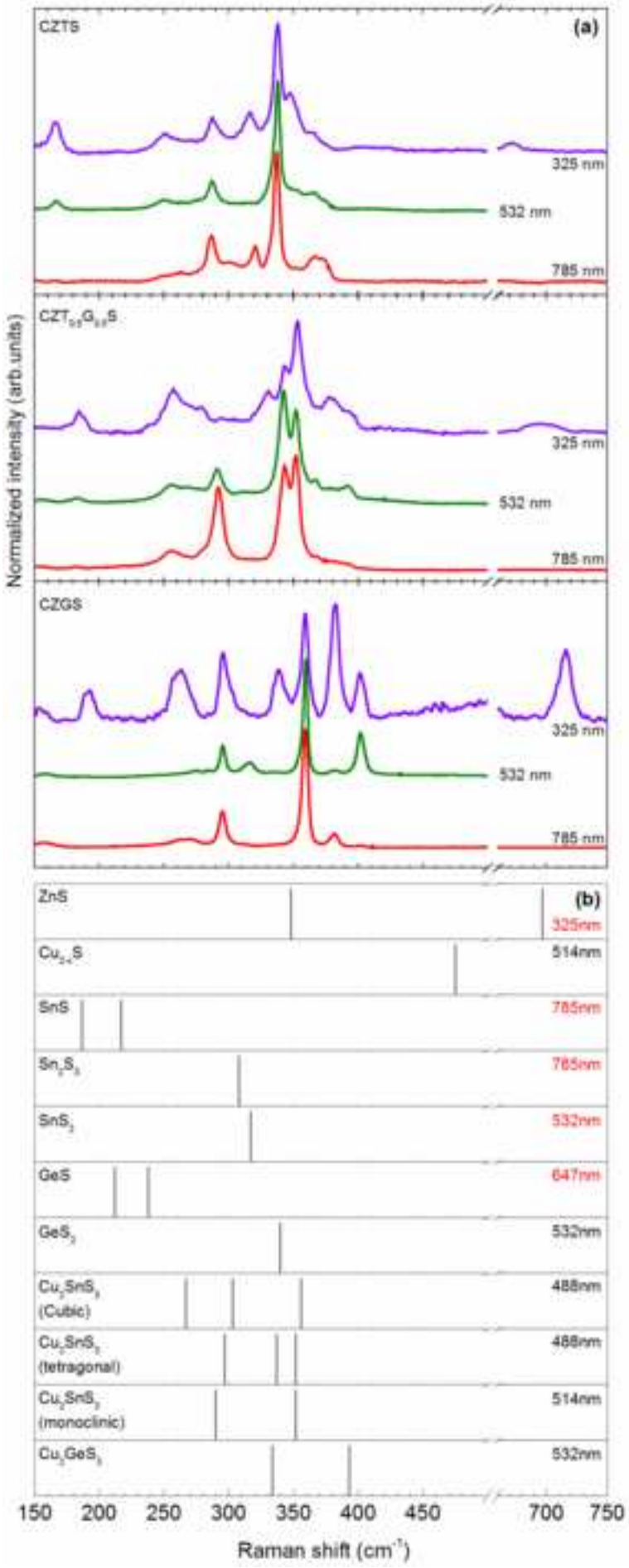

Figure
Click here to download high resolution image

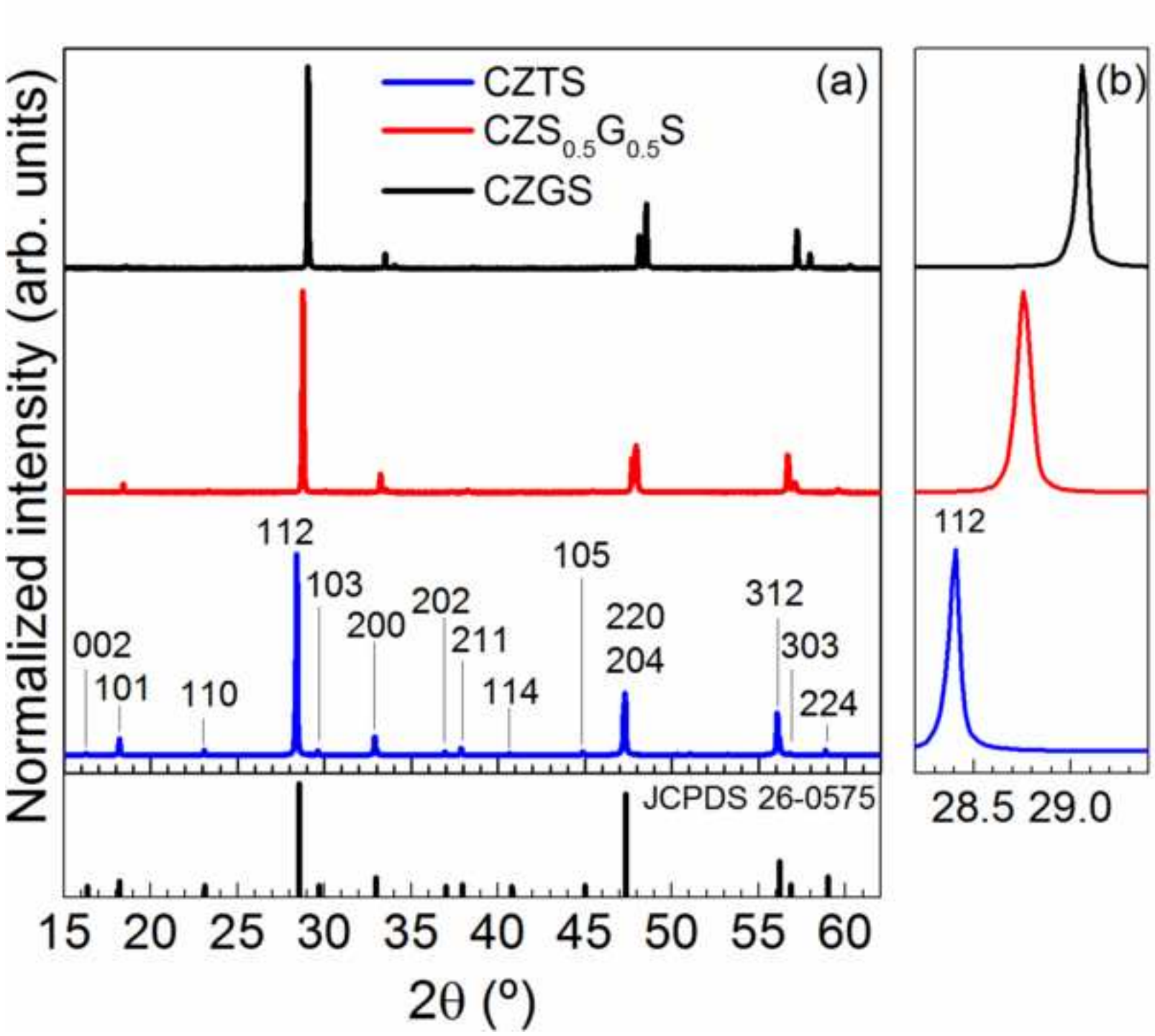

Figure
Click here to download high resolution image

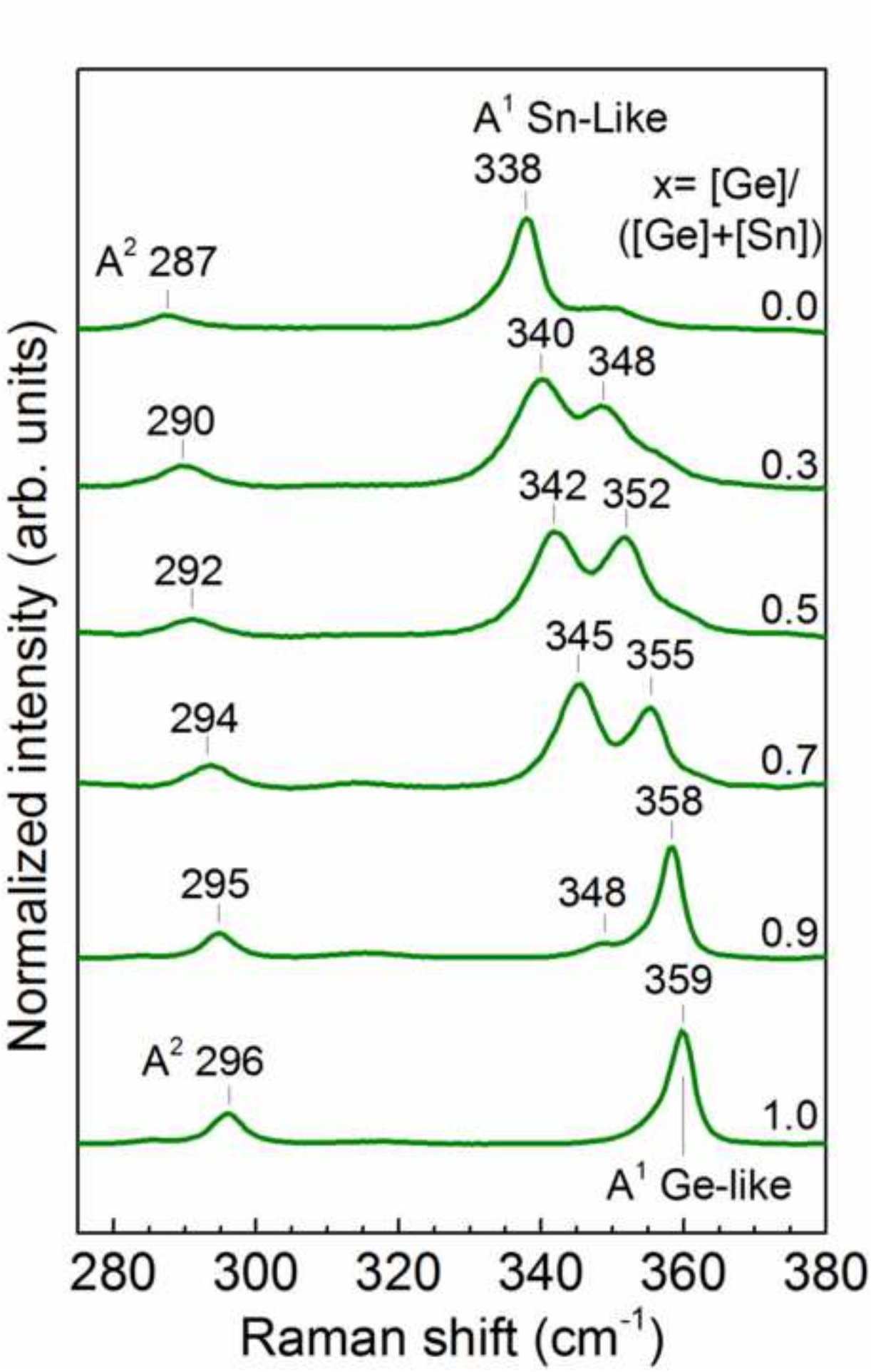

Figure
Click here to download high resolution image

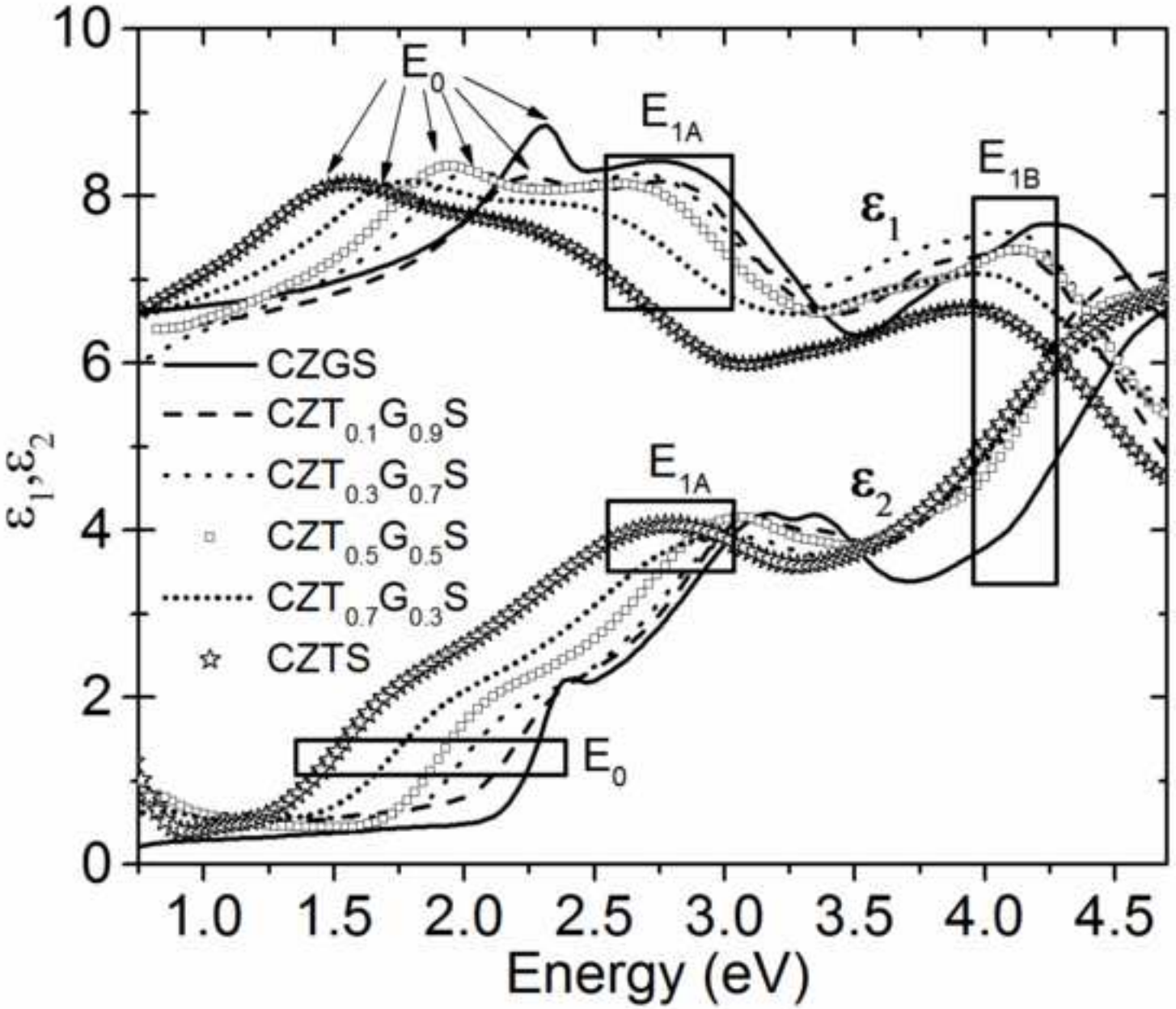

Figure

Click here to download high resolution image

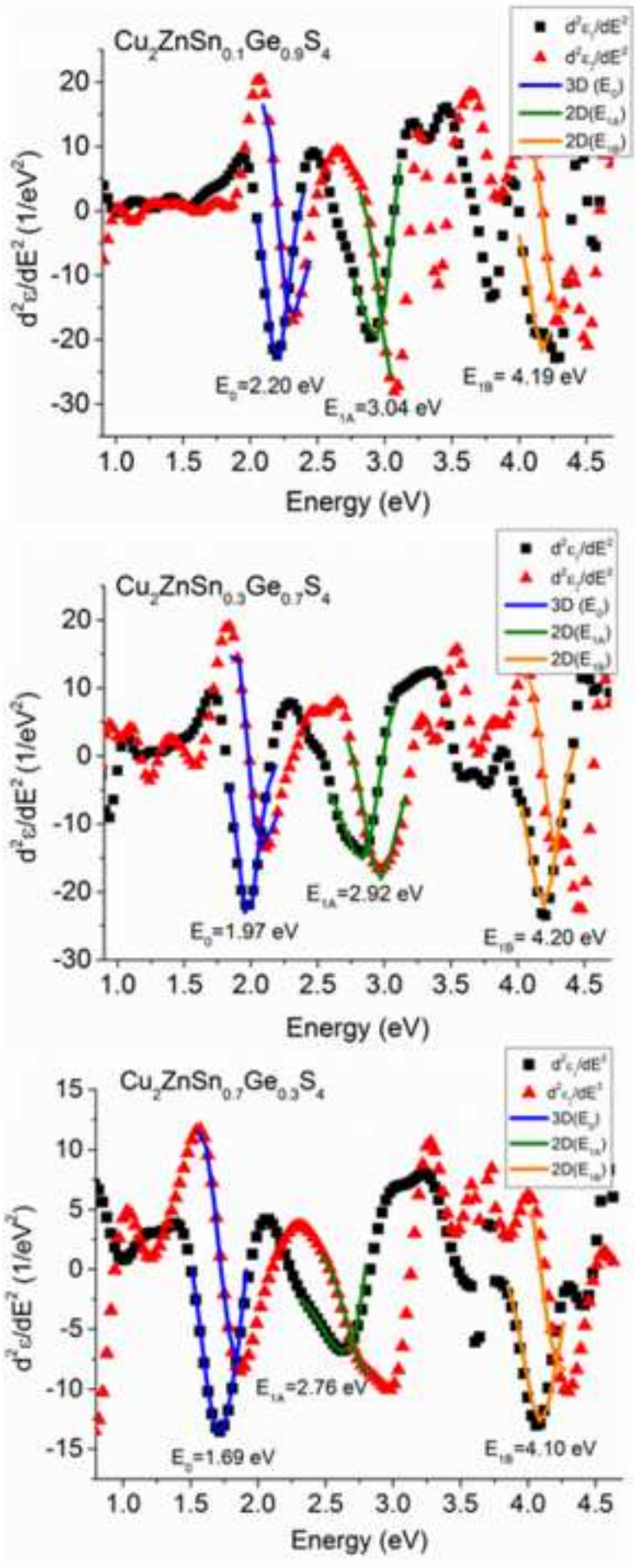

Figure
Click here to download high resolution image

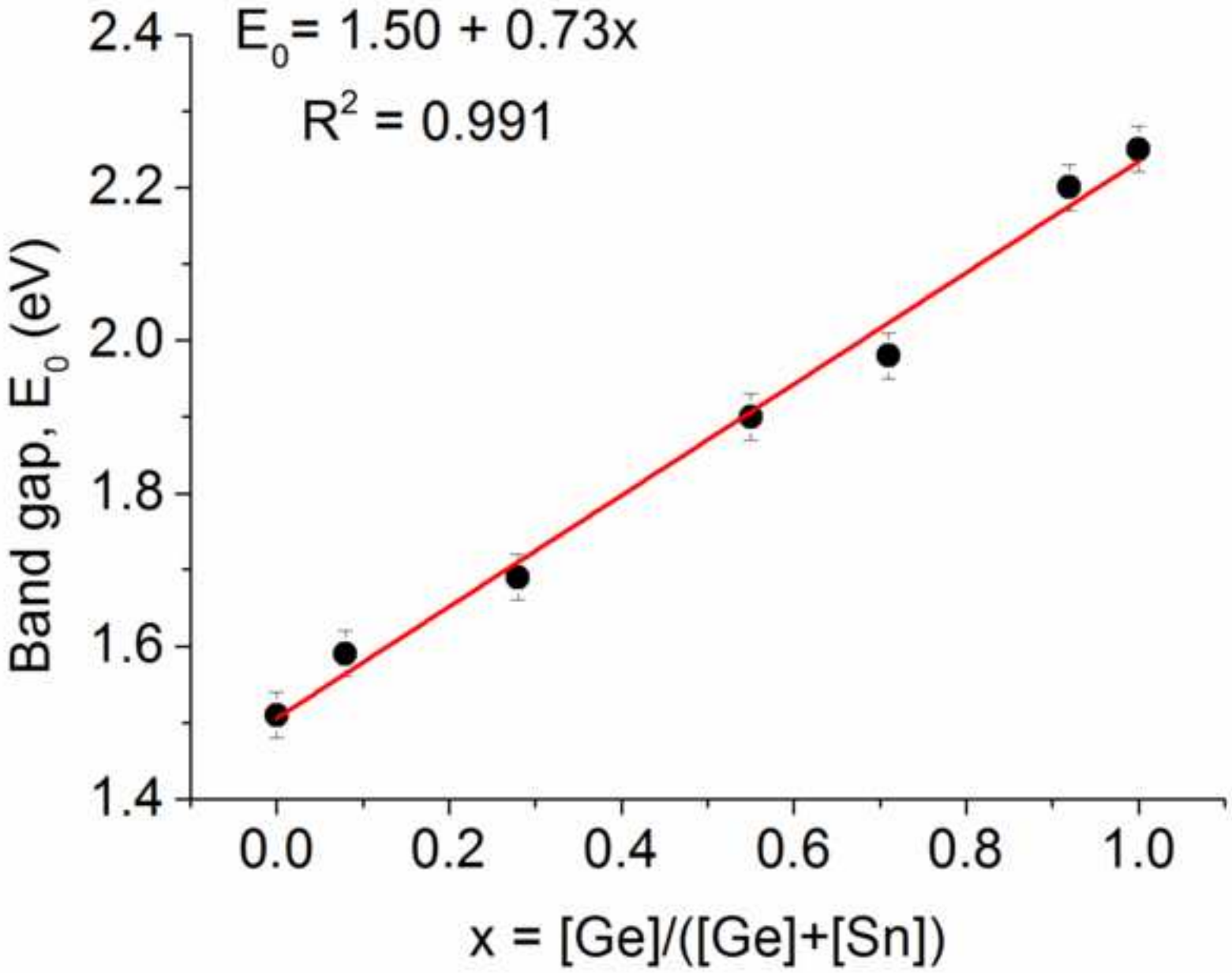

Figure Captions

Figure 1: (a) Raman spectra under 325, 532, and 785 nm excitation wavelengths for CZTS, $CZT_{0.5}G_{0.5}S$ and CZGS. (b) Summary of the reported main peaks for the possible secondary phases (ZnS [29], $Cu_{2-x}S$ [17,36] , SnS [16,34] , Sn_2S_3 [16,33], SnS_2 [32], GeS [35], GeS_2 [37], Cubic Cu_2SnS_3 [38], tetragonal Cu_2SnS_3 [32,38], monoclinic Cu_2SnS_3 [39], Cu_2GeS_3[40]). The red labels indicate the Raman spectra reported under resonant conditions.

Figure 2: X-Ray diffractogram of CZTS, CZT0.5G0.5S and CZGS single crystals (a), and detail of (112) plane (b).

Figure 3: Raman spectra detail of the A^2 and A^1 region under 532 nm excitation wavelength obtained for different x=[Ge]/([Ge]+[Sn]) compositions

Figure 4. Experimental spectral dependence of dielectric function $\varepsilon(E)= \varepsilon_1(E) + i\varepsilon_2(E)$ of $Cu_2ZnSn_{1-x}Ge_xS_4$ single crystals. The spectra exhibit three CP structures, E_0, E_{1A} and E_{1B} for each compound

Figure 5. Second derivative spectra of the experimental real and imaginary dielectric functions and the fitting based on equation (1) of $Cu_2ZnSn_{0.3}Ge_{0.7}S_4$, $Cu_2ZnSn_{0.7}Ge_{0.3}S_4$ and $Cu_2ZnSn_{0.9}Ge_{0.1}S_4$ single crystals. The transition energies E_0, E_{1A} and E_{1B} values are given.

Figure 6. Variation of the fundamental band gap energy with the x= [Ge]/([Sn]+[Ge]) atomic ratio. The solid line represents the linear fit of the experimental data.